Batteries & Supercaps

Research Article
doi.org/10.1002/batt.202400778

Chemistry Europe
European Chemical Societies Publishing

www.batteries-supercaps.org

Stabilizing Cathode-Electrolyte Interface by Low-Cost Ethyl Methylsulfone Co-Solvent for High-Voltage Sodium-ion Batteries

Xinran Hu,[a] Wenxi Hu,[a] Deda Peng,[a] Xiaowei Liu,[a] Xing Zhou,[a] Meilong Wang,[a] Yongyuan Zhou,[a] Jin Han,*[b] Tiefeng Liu,*[c, d] and Ya You*[a, b]

Raising the upper cut-off voltage of cathode is an effective method to improve the energy density of sodium-ion batteries (SIBs). However, the high upper cut-off voltage could cause severe side reactions and injure the cycle life of SIBs as the absence of stable cathode-electrolyte interface. Some fluorinated co-solvents have been ever employed and proven effective in stabilizing the cathode-electrolyte interface to support the normal operation of SIBs under a high upper cut-off voltage. However, the high-cost of fluorinated co-solvents would notably improve battery expenses. In this study, a low-cost co-solvent called ethyl methylsulfone (EMS) is introduced into the electrolyte for the $Na_{0.67}Mn_{0.8}Cu_{0.2}O_2$ cathode with a high upper cut-off voltage of 4.5 V. It is found that a stable and uniform cathode-electrolyte interface (CEI) forms on the cathode, which mitigates the cathode degradation and enhances the cycling stability of cathode. Consequently, this cathode with the designed electrolyte achieves a high capacity retention of 83.2% after 750 cycles at a current density of 1 C (1 C = 110 mAh g^{-1}). This work provides valuable insights into the development of electrolytes for sodium-ion batteries working at high-voltage.

Introduction

Sodium-ion batteries (SIBs) are attracting growing attention in the field of electrical energy storage due to the advantages in cost-saving, rate performance under low temperatures and safety over lithium-ion batteries.[1] However, the energy density of state-of-the-art SIBs still has promotion space for the practical application. Cathode materials play a crucial role on determining the energy density of SIBs. Among cathode materials, layered transition metal oxides (Na_xTMO_2, TM = transition metal, $x \leq 1$) have emerged as one of the most promising candidates due to their high energy, ease of synthesis, and abundant element resources.[2] To achieve higher energy, raising the upper cut-off voltage proves to be an effective approach, which can increase the average operating voltage and capacity.[3] Nevertheless, currently used commercial electrolytes for SIBs are prone to decomposition at the high voltage due to the formation of instable CEI and fail to sustain the operation of high-voltage cathode for SIBs.[4]

Many attempts have been devoted to improving the anodic electrochemical stability of the electrolyte by employing highly-concentrated electrolytes (HCE) and introducing co-solvents. The unique solvation structure in HCE indeed improve the anodic electrochemical stability of electrolytes.[5] However, the viscosity of HCE is sharply raised due to the increased salt concentration, resulting into the decreased ionic conductivity and poor wettability with electrode and separator. Moreover, HCE could raise the cost to some degree.[5c,6] In comparison with HCE, the introduction of co-solvents can not only reduce the concentration and enhance ionic conductivity of electrolyte, but also adjust the solvation structure and electrode/electrolyte interface.[7] Among these co-solvents, fluorinated solvents are the most commonly used, such as DFEC, TFPC and TFEC.[8] Nevertheless, these high-cost fluorinated solvents could improve the expense of electrolyte. Therefore, it is essential to explore some low-cost co-solvents to improve the anodic electrochemical stability of the electrolyte especially at the high voltage.[8a,9]

In this work, a fluoride-free compound, ethyl methylsulfonate (EMS, Figure S1), is proposed as a low-cost co-solvent to develop an electrochemically stale electrolyte at the high voltage. We formulate this electrolyte with a composition of 1 mol L^{-1} (M) $NaPF_6$ dissolved in blended solvents containing propylene carbonate (PC), EMS and fluoroethylene carbonate (FEC) with a volume ratio of 7: 3: 0.1 (denoted as PMF). The EMS can be preferentially decomposed to form an interface on the

[a] X. Hu, W. Hu, D. Peng, X. Liu, X. Zhou, M. Wang, Y. Zhou, Prof. Y. You
State Key Laboratory of Advanced Technology for Materials Synthesis and Processing
Wuhan University of Technology, Wuhan 430070, P. R. China
E-mail: youya@whut.edu.cn

[b] Prof. J. Han, Prof. Y. You
International School of Materials Science and Engineering, School of Materials Science and Microelectronics
Wuhan University of Technology, Wuhan 430070, P. R. China
E-mail: jinhan@whut.edu.cn

[c] Prof. T. Liu
College of Chemical and Biological Engineering
Zhejiang University, Hangzhou 310058, Zhejiang, China
E-mail: tiefengliu@zju.edu.cn

[d] Prof. T. Liu
Quzhou Institute of Power Battery and Grid Energy Storage
Quzhou 324000, Zhejiang, China

Supporting information for this article is available on the WWW under https://doi.org/10.1002/batt.202400778

Research Article
doi.org/10.1002/batt.202400778
Chemistry Europe
European Chemical Societies Publishing

cathode due to its higher highest occupied molecular orbital (HOMO) energy level. The designed electrolyte facilitates the formation of a stable, robust, and sulfate-rich interface on the cathode. This interface effectively inhibits the dissolution of transition metal ions from the cathode during the cycle process, significantly enhancing the cycle life of the Na||$Na_{0.67}Mn_{0.8}Cu_{0.2}O_2$ battery in the working potential range from 2 V to 4.5 V. Concretely, the battery with this electrolyte retains a capacity retention of 83.2% after 750 cycles at 1 C. This work offers insights on development of electrolyte for SIBs with high upper cut-off voltage.

Results and Discussion

Electrolyte Properties

Compared with a variety of fluorine-containing electrolytes, EMS as co-solvent has the advantage of low cost (Table S1). To know about physicochemical property of solvents utilized in this work, the highest occupied molecular orbital (HOMO) and the lowest unoccupied molecular orbital (LUMO) of the PC, EMS and FEC are further calculated based on the frontier molecular orbital theory. As shown in Figure 1a, EMS has a higher HOMO energy (−7.829 eV) than PC (−8.140 eV) and FEC (−8.702 eV), indicating that EMS loses electrons and is preferentially oxidized before the other two solvents. 1 M $NaPF_6$ in PC: FEC (1: 0.1, vol %) blended solvents, denoted as PF, is chosen as the reference electrolyte. The electrochemical stability of the PMF and PF electrolytes is evaluated through linear sweep voltammetry (LSV) test at a scan rate of 5 mV s^{-1}. Actually, Al foil has been used as the working electrode for the LSV test at the beginning, and the oxidation current is obviously raised at 3.2 V in PMF electrolyte in Figure S2a, indicating the electrochemical reaction between Al foil and PMF electrolyte. So, the plateaus at 3.2 V in the charge–discharge curves of battery could be caused by the above-mentioned reaction between Al foil and PMF electrolyte. As comparison, there is no obvious oxidation current until 4.2 V for Ti current collector as result of its outstanding electrochemical stabilization in Figure S2b. Meanwhile, the Ti foil is used as the current collector of cathode in the battery preparation. It demonstrates that the plateaus at 3.2 V and the large irreversible capacity disappears in Figure S3. This phenomenon keeps consistent with results of the calculated LUMO and HOMO energy levels in Figure 1a. The preferential decomposition of EMS lays the foundation for the formation of a stable interface in the PMF electrolyte.

To further investigate the working mechanism of EMS in the PMF electrolyte, we analyze the interactions and solvation structures of each component. As shown in Figure 1b, a characteristic peak at 1166 cm^{-1} is assigned to the sulfur-oxygen double bond (S=O) in EMS. The S=O characteristic peak does not exhibit a blue shift in the mixed solution of EMS and FEC, indicating that there is no interaction between EMS and FEC. In contrast, a blue shift of the S=O peak is noted in the mixed solution of EMS and PC at 1172.7 cm^{-1}, suggesting that the interaction between PC and EMS affected the local environment of EMS. Furthermore, the S=O peak shows a greater blue shift in the PMF electrolyte at 1176 cm^{-1} compared to the mixed solution of EMS and PC, indicating that the chemical environment around EMS molecules has changed and EMS interacts with Na^+ ion and PC. Additionally, molecular dynamics

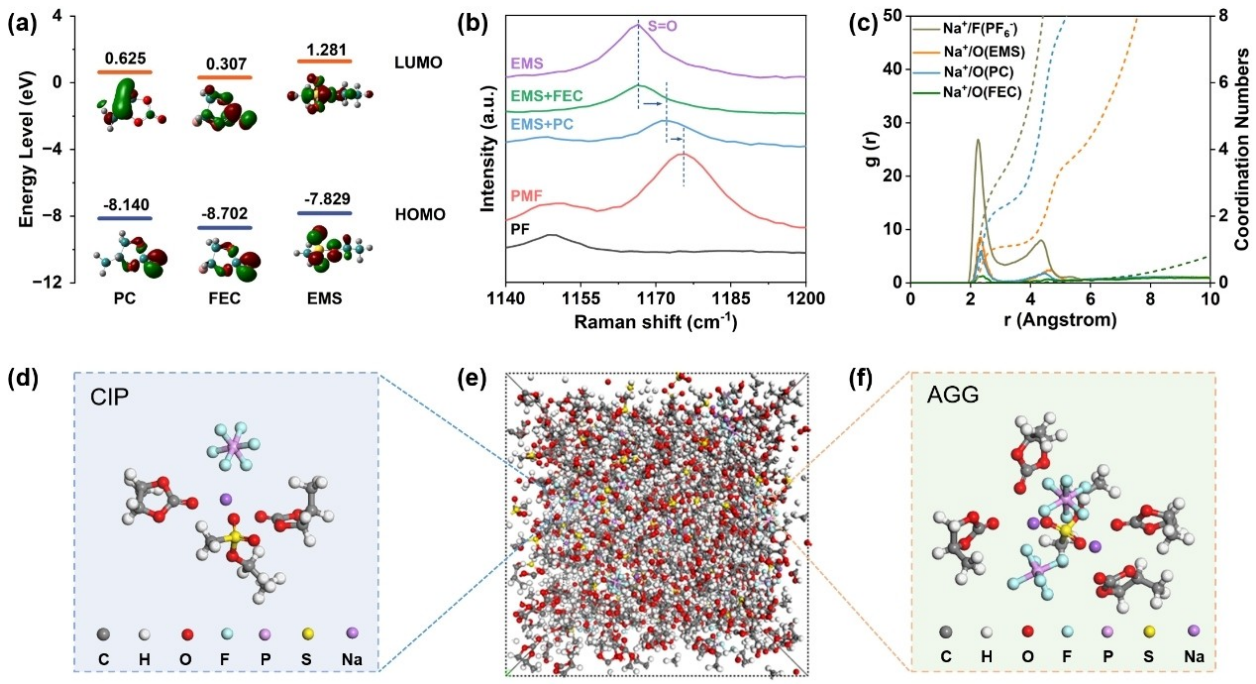

Figure 1. The theoretical analysis of electrolyte solvation structure. (a) The LUMO/HOMO energy level diagram for PC, FEC, and EMS molecule. (b) Raman spectra of EMS, EMS + FEC and EMS + PC solvent, and EMS + $NaPF_6$, PMF and PF electrolyte. (c, e) RDF results of Na^+ and Snapshot acquired from MD simulations of PMF electrolyte. (d, f) Locally enlarged solvation structure acquired from MD simulations of PMF electrolyte.

Research Article
doi.org/10.1002/batt.202400778
Chemistry Europe
European Chemical Societies Publishing

(MD) simulations further validate the solvation structure of the PMF electrolyte (Figure 1c–1f). The selected snapshots and analysis of the radial distribution function (RDF) reflected the solvation structure of between Na^+ cations and PC, EMS, FEC, primarily consisting of contact ion pairs (CIPs) and aggregated species (AGGs). The coordination number between Na^+ and PC is 2.25, while the coordination number between Na^+ and EMS is 1.08, confirming that EMS participates in the solvation structure of the PMF electrolyte.

Electrochemical Performance of Na||$Na_{0.67}Mn_{0.8}Cu_{0.2}O_2$ Cell

In order to select the optimal ratio of PC and EMS, the cell is equipped with the electrolyte having the different volume ratio of PC and EMS (7/3, 1/1, and 3/7). As shown in Figure S4 and Table S2, the cell has the optimal performance when the volume ratio of PC and EMS is 7:3.

To reveal the impact of the EMS solvent on the cycling performance of Na||$Na_{0.67}Mn_{0.8}Cu_{0.2}O_2$ cells, the cells employing PMF and PF electrolytes are measured through galvanostatic cycling at 0.3 C in different voltage ranges. As shown in Figure 2a and 2d, the cycling performance of the battery is similar in the cells with both PF and PMF electrolytes in the voltage range of 2–4 V. However, when the upper cutoff voltage is increased from 4 V to 4.5 V, as illustrated in Figures 2b and 2e, the specific capacity of the battery in the PMF electrolyte significantly increases by approximately 17%. After 150 cycles in the PMF electrolyte, the capacity retention of the cell is about 91%, which is higher than that in the PF electrolyte approximately 86%. Notably, in the case of low rate, the cell working in the PF electrolyte overcharges, because the electrolyte is prone to violent side-reactions. It is worth noting that the cell with the PMF electrolyte has an oxidation platform in the second cycle. As shown in Figure S5, the second charge cycle of the cell with PMF electrolyte exhibits a specific capacity of 262.6 mAh g^{-1} at 2–4.5 V, with a platform observed at 3.2 V. Similarly, a platform can also be observed at the 3.2 V when the cell works in range of 2–4 V, which may be attributed to the oxidation of the EMS solvent in the electrolyte.

The reduction and oxidation peak at around 4 V belongs to Cu^{2+}/Cu^{3+} in the cyclic voltammetry (CV). The voltage gap (ΔV)

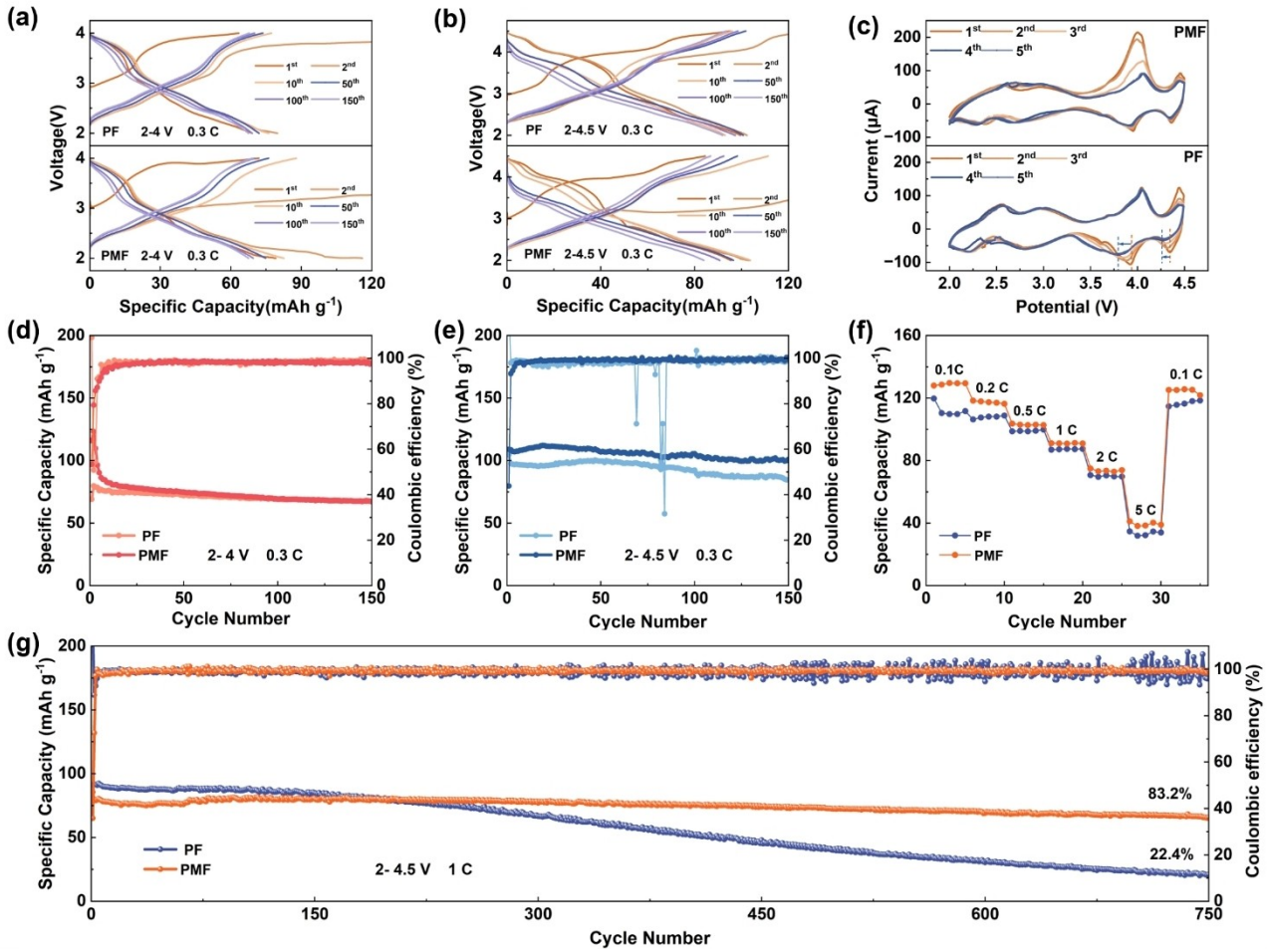

Figure 2. Galvanostatic charge–discharge profiles of Na||$Na_{0.67}Mn_{0.8}Cu_{0.2}O_2$ cells over different cycles at 0.3 C with the PMF and PF electrolyte across different voltage ranges: (a) 2–4 V and (b) 2–4.5 V. (c) Cyclic voltammetry of the $Na_{0.67}Mn_{0.8}Cu_{0.2}O_2$ cathode material in PMF and PF electrolyte. Cycling performance of Na||$Na_{0.67}Mn_{0.8}Cu_{0.2}O_2$ cells at 0.3 C across different voltage ranges: (d) 2–4 V and (e) 2–4.5 V. (f) Rate capability of Na||$Na_{0.67}Mn_{0.8}Cu_{0.2}O_2$ cell. (g) Cycling performance of Na||$Na_{0.67}Mn_{0.8}Cu_{0.2}O_2$ cells with a working voltage range from 2 to 4.5 V at 1 C.

Research Article
doi.org/10.1002/batt.202400778
Chemistry Europe
European Chemical Societies Publishing

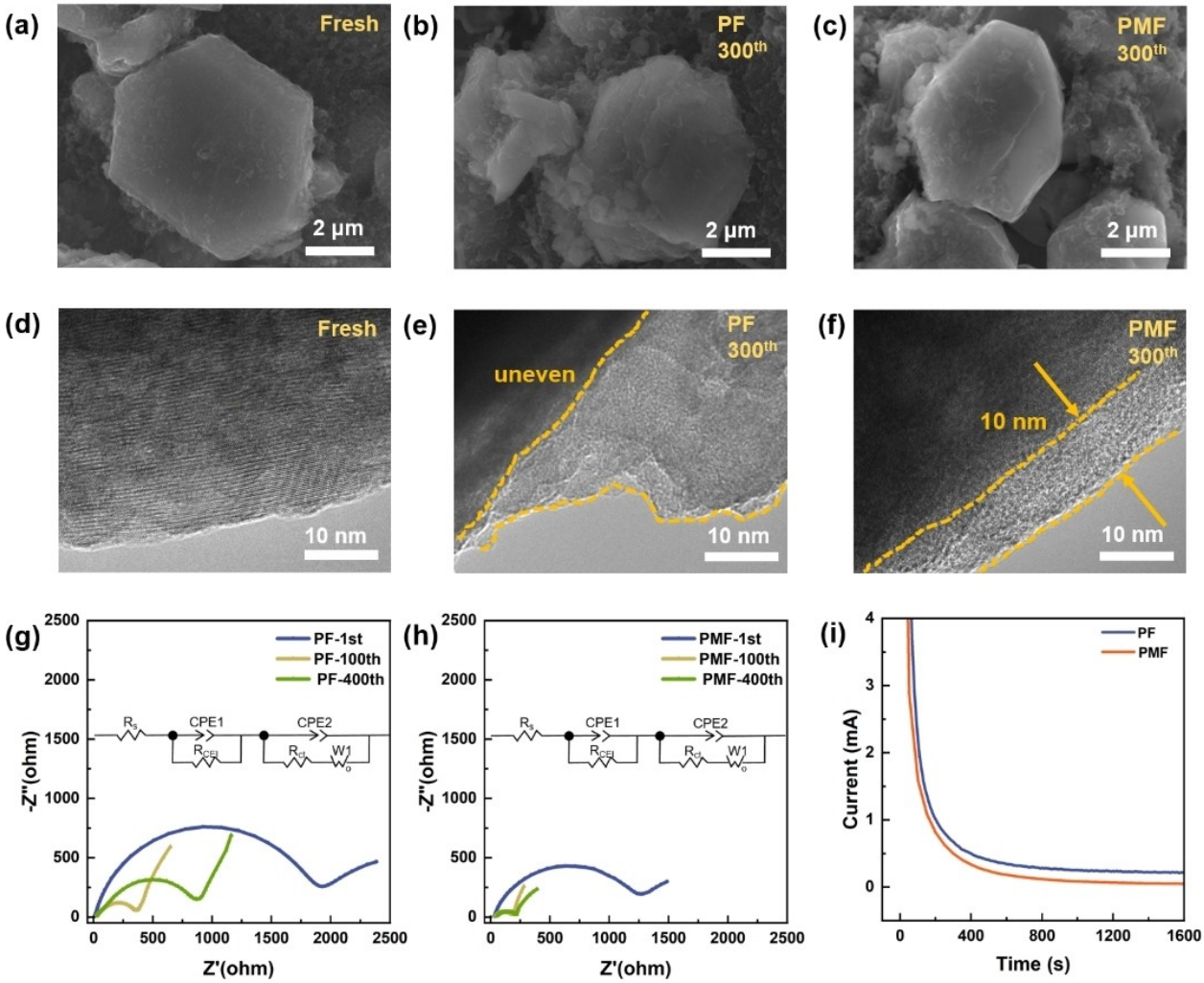

Figure 3. SEM and TEM images of fresh $Na_{0.67}Mn_{0.8}Cu_{0.2}O_2$ (a, d) and the $Na_{0.67}Mn_{0.8}Cu_{0.2}O_2$ cathodes cycled in PF electrolyte (b, e) and PMF electrolyte (c, f) for 300 cycles at 1 C with an upper charge cutoff voltage of 4.5 V. (g, h) Nyquist plots of Na||$Na_{0.67}Mn_{0.8}Cu_{0.2}O_2$ cells with (g) PF and (h) PMF electrolytes after 1, 100 and 400 cycles. (i) Chronoamperometry (floating charge) test.

between the reduction and oxidation peaks reflects the kinetics behavior of Na^+ insertion/extraction. As shown in Figure 2c, ΔV in the PMF electrolyte is 42.7 mV, much smaller than that in PF electrolyte (126 mV), indicating that the voltage polarization of the battery is more serious in the PF electrolyte. With the increase of the number of cycles, the ΔV in the PF electrolyte continuously rises while the ΔV in PMF electrolyte remains stable, demonstrating that the reversibility of redox reaction in the battery is reduced. Rate performance of Na||$Na_{0.67}Mn_{0.8}Cu_{0.2}O_2$ cells is measured in the PMF and PF electrolyte at different current densities. As shown in Figure 2f, the discharge capacities of the cell with the PMF electrolyte at 0.1, 0.2, 0.5, 1, 2, and 5 C are 129.4, 117.8, 102.9, 91.2, 73.5, and 40.3 mAh g^{-1}, respectively, which are higher than that of in the PF electrolyte. When the current density returns to 0.1 C, the capacity of the cell can almost recover to its initial capacity (125.6 mA h g^{-1}) in the PMF electrolyte, indicating better rate capability of cathode in the PMF electrolyte.

As shown in Figure 2g and Figure S6, the cell with PF electrolyte delivers an initial capacity of 91.35 mAh g^{-1}, and the capacity quickly drops to 21.36 mAh g^{-1} with a capacity retention of 22.40% after 750 cycles accompanied by fluctuating coulombic efficiency (CE) between 95% and 105%. Aside from the capacity retention, the increase in voltage polarization can be obviously observed. The sharp capacity decay and the fluctuation of CE are attributed to the poor electrochemical stability of PF electrolyte. In contrast, the initial capacity of the cell with PMF electrolyte is 85.49 mAh g^{-1} and the battery capacity remained at 65.68 mAh g^{-1} with a capacity retention of 83.22% after 750 cycles. In addition, the CE of the cell with PMF electrolyte gradually remains stable after 10 cycles with an average CE of 99.12%.

Research Article
doi.org/10.1002/batt.202400778
Chemistry Europe
European Chemical Societies Publishing

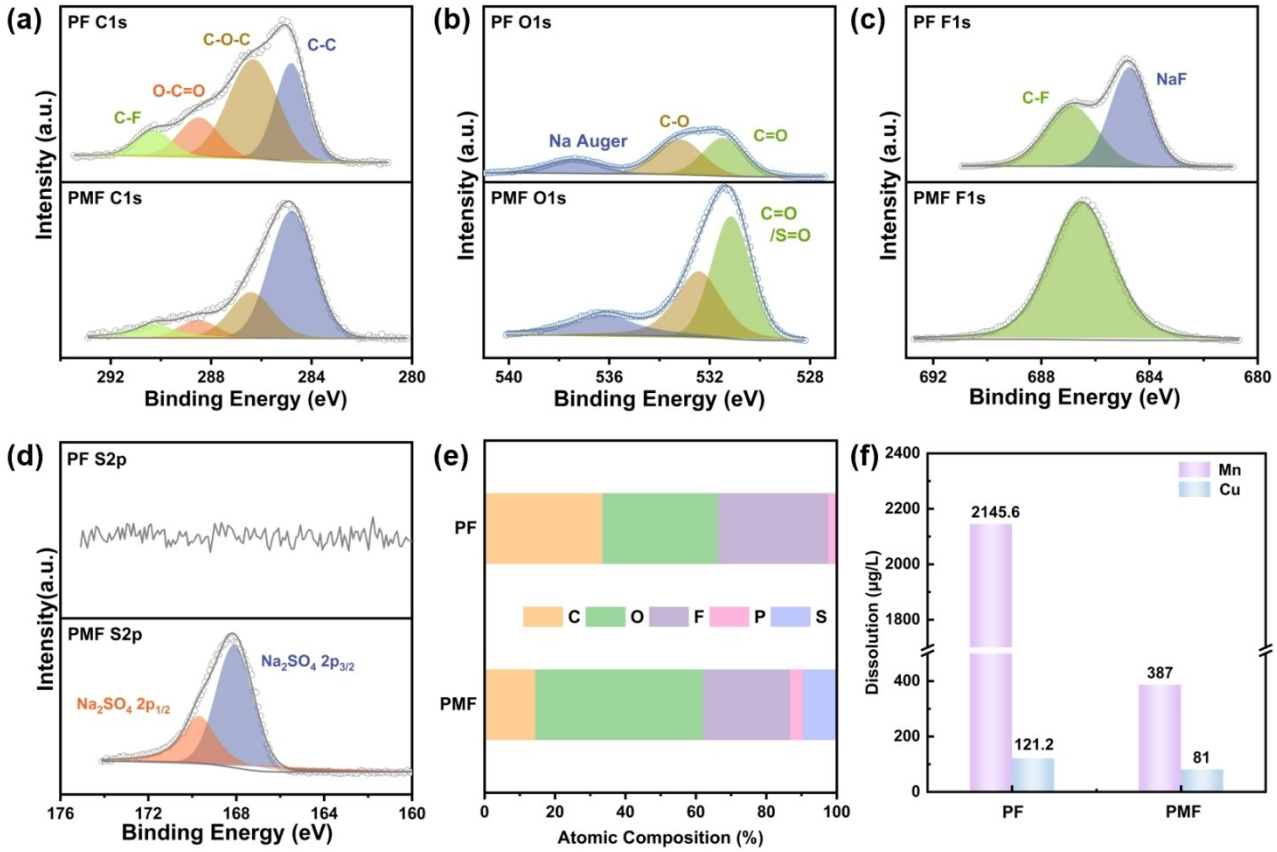

Figure 4. XPS characterization of CEI on the cathode after 300 cycles in PF and PMF electrolytes. (a) C 1s, (b) O 1s, (c) F 1s, (d) S 2p spectra. (e) Relative content of elements. (f) The amounts of Mn and Cu element escaped from $Na_{0.67}Mn_{0.8}Cu_{0.2}O_2$ cathodes after cycling in different electrolytes (for 300 cycles).

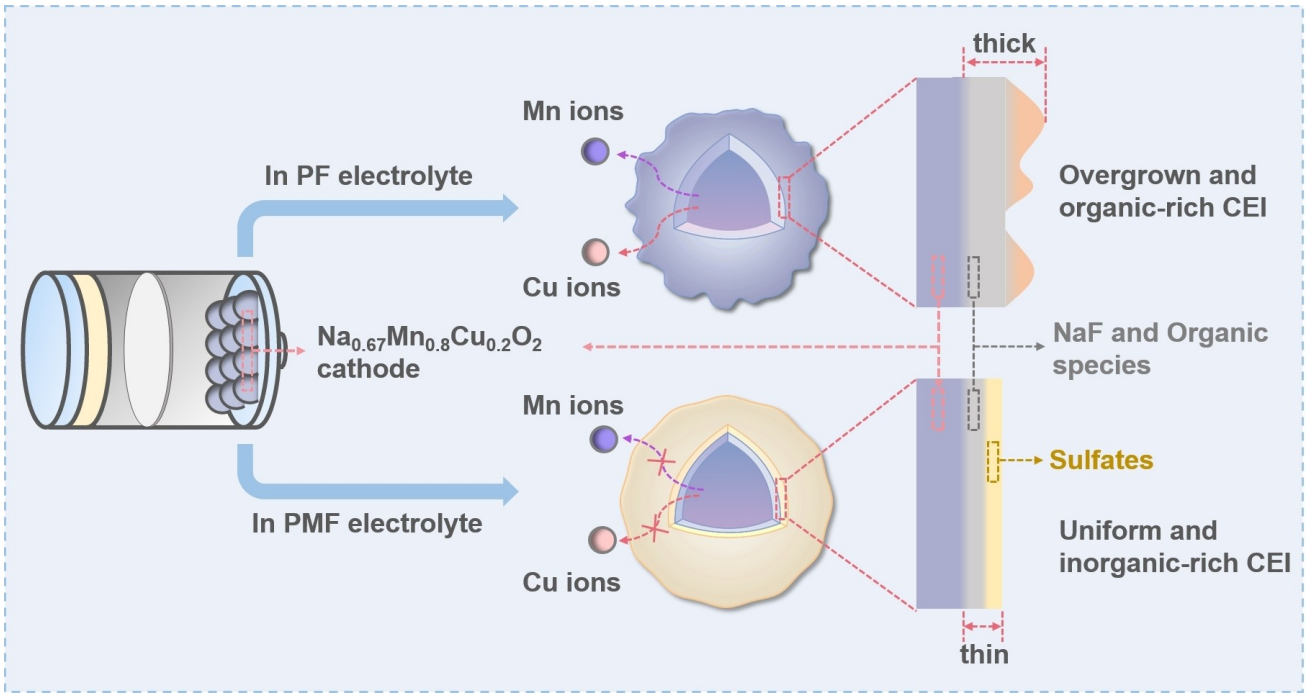

Figure 5. Schematic illustration for the working mechanism of selected electrolyte on the $Na_{0.67}Mn_{0.8}Cu_{0.2}O_2$ cathode.

Interface Analysis and Working Mechanism

To understand the effects of two electrolytes on the electrochemical performance of the cathode, Scanning Electron Microscopy (SEM), Transmission Electron Microscopy (TEM), and X-ray Photoelectron Spectroscopy (XPS) are performed on the cathodes after 300 cycles in Na||$Na_{0.67}Mn_{0.8}Cu_{0.2}O_2$ cells. Figure 3a–3c shows the SEM images of the fresh and cycled $Na_{0.67}Mn_{0.8}Cu_{0.2}O_2$ cathodes with the PF and the PMF electrolytes. Before cycling, the clean and smooth surface is clearly displayed on fresh $Na_{0.67}Mn_{0.8}Cu_{0.2}O_2$ electrode in Figure 3a. However, after 300 cycles, the cathode structure cycled in the PF electrolyte becomes fragmented (Figure 3b). This phenomenon can be attributed to the inadequate protection by the CEI layer in PF electrolyte during cycling process. In contrast, the cathode structure remained well-preserved in the PMF electrolyte even after 300 cycles (Figure 3c).

To further prove the effect of EMS solvent on the protection of $Na_{0.67}Mn_{0.8}Cu_{0.2}O_2$ cathode, TEM characterizations are carried out. The fresh electrode shows a clean surface as depicted in Figure 3d. However, the cathode surface becomes covered with an uneven thickness of CEI layer after undergoing 300 cycles in the PF electrolyte (Figure 3e). By contrast, the cathode surface is endowed with a dense and uniform CEI layer of approximately 10 nm thickness by using PMF electrolyte (Figure 3f). This difference unequivocally demonstrates that the introduction of EMS promotes the formation of a thin CEI layer under high voltage conditions, effectively preventing undesirable reactions between the electrolyte and electrode components to further ensure excellent cyclic stability.

To verify whether the CEI layer formed from the EMS solvent has superior Na^+ ion transport kinetics, electrochemical impedance spectroscopy (EIS) test is performed on the cells with the PF and PMF electrolyte. Nyquist plots of $Na_{0.67}Mn_{0.8}Cu_{0.2}O_2$ cathode cycled in PMF and PF electrolytes are collected in Figure 3g and Figure 3h. EIS results are fitted by an equivalent electric circuit, where R_s, R_{ct} and R_{CEI} represent ohmic resistance, the charge-transfer resistance, and the resistance of Na^+ through the interface, respectively. The R_{CEI} of cells utilizing the PMF electrolyte after 1, 100, 400 cycles are 1239.6 Ω, 146.9 Ω and 162.2 Ω, respectively. And the R_{CEI} of cells utilizing the PF electrolyte after 1, 100, 400 cycles are 1914.3 Ω, 337.8 Ω and 852.3 Ω, respectively. The smaller impedance is beneficial to accelerate the transport kinetics. As shown in Figure 3g and 3 h, the cells with the PMF electrolyte effectively reduce the impedance, indicating that the CEI formed by PMF electrolyte has better reaction kinetics. The higher R_{CEI} of the PF electrolyte could be attributed to the thick CEI layer formed by the decomposition of the electrolyte, which slows down ion transport through the interface. Galvanostatic intermittent titration technique (GITT) test was further conducted to evaluate the ionic diffusion coefficient of the cells with two different electrolytes (Figure S7). The high ion diffusion coefficient in both electrolytes demonstrates superior Na^+ ion diffusion kinetics in the battery. The chronoamperometry (floating charge) test was exerted to monitor the leakage current of $Na_{0.67}Mn_{0.8}Cu_{0.2}O_2$ at upper charge cut-off voltage in the PF and PMF electrolytes. The leakage current density of the cell in the PMF electrolyte is apparently below that in the PF electrolyte (Figure 3i). The rapidly diminishing leakage current indicates that the CEI layer on the cathode with the PMF electrolyte could effectively protect the surface of the cathode and inhibit the side reactions at the interface at high voltages. The larger leakage current density monitored in the PF electrolyte implies the severe side reactions between the electrolyte and the cathode.

To further reveal the effect of PF and PMF electrolytes on the interface, the cycled electrodes are analyzed by XPS. The full XPS spectra for the cycled electrodes with the PMF and the PF electrolytes are displayed in Figure S8. For the C1s spectra (Figure 4a), the C–C peak at 284.8 eV belongs to the conductive carbon peak, while the C–O–C peak at 286 eV and the O–C=O peak at 288.5 eV are derived from the decomposition of organic carbonate solvents.[10] The C–F peak at 291 eV is regarded as PVDF binder. It is worth noting that the peak intensities of C–O–C and O–C=O in PMF electrolyte are much weaker than that in PF electrolyte, indicating more organic products after decomposition on the electrode with PF electrolyte. The position of 532.0 eV in Figure 4b corresponds to the C=O and S=O bonds, indicating that the CEI contains sulfur-containing conpounds as result of EMS decomposition.[11] S 2p is also the characteristic spectrum of in PMF electrolyte. As shown in Figure 4d, peaks at 168 eV and 170 eV assigned to Na_2SO_4 $2p_{3/2}$ and Na_2SO_4 $2p_{1/2}$, respectively, demonstrates Na_2SO_4 in CEI derives from the decomposition of EMS solvents.[12] As a primary decomposition product of EMS, Na_2SO_4 is naturally insoluble and has highly oxidation stability.[13] In the F1s spetrum (Figure 4c), NaF peak (684~685.5 eV) is attributed to the decomposition of FEC.[5b] There is only C–F (≈688.0 eV) in the cathode with PMF electrolyte, corresponding to PVDF binder. Combined with the etching diagrams of fluorine and sulfur in Figures S9 and S10, there is no sodium fluoride on the surface of CEI formed with the PMF electrolyte. As the etching depth increases, the increased NaF and decreased Na_2SO_4 indicate that CEI is formed by oxidation of sulfur-containing compounds in the solvent, while fluoride is not decomposed. Thereby, the consumption of other solvents is obviously reduced. Furthermore, lower Mn radio is detected at the $Na_{0.67}Mn_{0.8}Cu_{0.2}O_2$ surface after cycling in the PMF electrolyte, indicating the formation of a compact CEI derived from EMS (Figures S11). By contrast, the increased exposure of Mn on the CEI layer formed with the PF electrolyte demonstrates poor integrity at the cathode surface. These results further confirm that the inorganic-rich and uniform CEI layer is constructed in the designed electrolyte using EMS as a co-solvent. Additionally, the ICP-OES (Inductively Coupled Plasma Optical Emission Spectroscopy) results presented in Figure 4f demonstrate a reduced leaching of transition metal ion in electrodes utilizing PMF electrolyte. The intensity of all elements is normalized to evaluate their relative content in the CEI layer (Figure 4e). The relative content of F, P, and S in the PMF electrolyte is significantly higher than those in the PF electrolyte, but the content of O and C is less in the PMF electrolyte. After a sum-up of inorganic species in the PMF electrolyte (Figure S12),

inorganic species in the PMF electrolyte is higher in comparison with the PF electrolyte.

The schematic illustration for the working mechanism of two electrolytes on the $Na_{0.67}Mn_{0.8}Cu_{0.2}O_2$ cathode is shown in Figure 5. The cathode working with PMF electrolyte generates an inorganic-rich and uniform CEI after cycling, which protects the cathode material from structure failure. In contrast, an overgrown and organic-rich CEI is formed on the cathode in the PF electrolyte, leading to the degradation of the cathode material and poor cycle life.

Conclusions

In summary, we have developed a novel electrolyte for SIBs by introducing a low-cost sulfonate solvent as the co-solvent, which exhibits a remarkable anodic electrochemical stability and enables the cathode with a high capacity retention at a high upper cut-off voltage condition. Concretely, the capacity retention of the assembled Na||$Na_{0.67}Mn_{0.8}Cu_{0.2}O_2$ cell with the designed electrolyte is 83.2% after 750 cycles in the voltage range of 2–4.5 V, whereas the capacity retention of PF electrolyte is only 22.4% after 750 cycles. This improvement is mainly attributed to inorganic-rich and uniform CEI on the cathode with the PMF electrolyte. The stable CEI layer inhibit the Mn ions and Cu ions dissolution and stabilize the structure of $Na_{0.67}Mn_{0.8}Cu_{0.2}O_2$. This work broadens the horizon to develop electrolytes with high anodic electrochemical stability for SIBs.

Acknowledgements

This work was supported by National Key Research and Development Program of China (2023YFB2406100) and the National Natural Science Foundation of China (Grant No. 52302306).

Conflict of Interests

The authors declare no conflict of interest.

Data Availability Statement

The data that support the findings of this study are available from the corresponding author upon reasonable request.

Keywords: low cost co-solvent · cathode electrolyte interface · sodium-ion batteries · high-voltage

[1] a) J.-Y. Hwang, S.-T. Myung, Y.-K. Sun, *Chem. Soc. Rev.* **2017**, *46*, 3529–3614; b) P. K. Nayak, L. T. Yang, W. Brehm, P. Adelhelm, *Angew. Chem. Int. Ed.* **2018**, *57*, 102–120; c) C. Yang, S. Xin, L. Mai, Y. You, *Adv. Energy Mater.* **2020**, *11*, 2000974; d) N. Yabuuchi, K. Kubota, M. Dahbi, S. Komaba, *Chem. Rev.* **2014**, *114*, 11636–11682.
[2] a) S. Li, Y. Sun, Y. Pang, S. Xia, T. Chen, H. Sun, S. Zheng, T. Yuan, *Asia-Pac. J. Chem. Eng.* **2022**, *17*, e2762; b) Q. Liu, Z. Hu, M. Chen, C. Zou, H. Jin, S. Wang, S. L. Chou, S. X. Dou, *Small* **2019**, *15*, 1805381; c) H. Liu, X. Gao, J. Chen, J. Gao, H. Wang, Y. Mei, H. Liu, W. Deng, G. Zou, H. Hou, X. Ji, *J. Energy Chem.* **2022**, *75*, 478–485; d) K. Chen, M. Lei, Z. Yao, Y. Zheng, J. Hu, C. Lai, C. Li, *Sci. Adv.* **2021**, *7*, eabj1491.
[3] a) W. Li, B. Song, A. Manthiram, *Chem. Soc. Rev.* **2017**, *46*, 3006–3059; b) Z. Wu, C. Cao, X. Yan, X. Zang, Y. Zhao, X. Ma, R. Liu, L. Hu, Y. Jiang, S. Sun, *Electrochim. Acta* **2019**, *302*, 153–160; c) L. Sun, J. Zeng, X. Wan, C. Peng, J. Wang, C. Lin, M. Zhu, J. Liu, *Electron* **2024**, *2*, e31; d) Y. Jiang, X. Hu, *Electron* **2023**, *1*, e15.
[4] a) X. Fan, C. Wang, *Chem. Soc. Rev.* **2021**, *50*, 10486–10566; b) C.-C. Su, M. He, J. Shi, R. Amine, Z. Yu, L. Cheng, J. Guo, K. Amine, *Energy Environ. Sci.* **2021**, *14*, 3029–3034; c) L. Huang, F. Makhlooghiazad, L. A. O'Dell, P. C. Howlett, M. Forsyth, *Mater. Adv.* **2024**, *5*, 6899–6909.
[5] a) T. Zheng, B. Zhu, J. Xiong, T. Xu, C. Zhu, C. Liao, S. Yin, G. Pan, Y. Liang, X. Shi, H. Zhao, R. Berger, Y.-J. Cheng, Y. Xia, P. Müller-Buschbaum, *Energy Storage Mater.* **2023**, *59*, 102782; b) C. Yang, X. Liao, X. Zhou, C. Sun, R. Qu, J. Han, Y. Zhao, L. Wang, Y. You, J. Lu, *Adv. Mater.* **2023**, *35*, 2210966; c) S. Lee, B. Koo, S. Kang, H. Lee, H. Lee, *Chem. Eng. J.* **2021**, *425*, 130612; d) Y. Yu, C. Lai, M. Lei, K. Chen, C. Li, *Mater. Horiz.* **2024**, *11*, 2169–2179.
[6] H. J. Liang, Z. Y. Gu, X. X. Zhao, J. Z. Guo, J. L. Yang, W. H. Li, B. Li, Z. M. Liu, W. L. Li, X. L. Wu, *Angew. Chem. Int. Ed.* **2021**, *60*, 26837–26846.
[7] a) Y. Chen, Y. Zhao, A. Wang, D. Zhang, B. Li, X. He, X. Fan, J. Liu, *Energy Environ. Sci.* **2024**, *17*, 6113–6126; b) J. Zhou, Y. Wang, J. Wang, Y. Liu, Y. Li, L. Cheng, Y. Ding, S. Dong, Q. Zhu, M. Tang, Y. Wang, Y. Bi, R. Sun, Z. Wang, H. Wang, *Energy Storage Mater.* **2022**, *50*, 47–54.
[8] a) H. Ren, G. Zheng, Y. Li, S. Chen, X. Wang, M. Zhang, W. Zhao, H. Yi, W. Huang, J. Fang, T. Liu, L. Yang, M. Liu, Q. Zhao, F. Pan, *Energy Environ. Sci.* **2024**, *17*, 7944–7957; b) M. He, C.-C. Su, C. Peebles, Z. Zhang, *J. Electrochem. Soc.* **2021**, *168*, 010505; c) K. Chen, W. Qiu, M. Lei, C. Lai, J. Liu, C. Li, *Matter* **2024**, *7*, 3906–3931.
[9] a) X. Jian, X. Liu, C. Yang, J. Xie, W. Hu, Y. Zhang, H. Yan, J. Han, Y. You, *Small* **2024**, *20*, 2400709; b) L. Yin, M. Wang, C. Xie, C. Yang, J. Han, Y. You, *ACS Appl. Mater. Interfaces* **2023**, *15*, 9517–9523; c) M. Qin, Z. Zeng, F. Ma, C. Gu, X. Chen, S. Cheng, J. Xie, *ACS Energy Lett.* **2024**, *9*, 2536–2544; d) Y. Wang, Z. Li, Y. Hou, Z. Hao, Q. Zhang, Y. Ni, Y. Lu, Z. Yan, K. Zhang, Q. Zhao, F. Li, J. Chen, *Chem. Soc. Rev.* **2023**, *52*, 2713–2763.
[10] X. F. Guo, Z. Yang, Y. F. Zhu, X. H. Liu, X. X. He, L. Li, Y. Qiao, S. L. Chou, *Small Methods* **2022**, *6*, 2200209.
[11] B. N. Olana, S.-H. Pan, B.-J. Hwang, H. Althues, J.-C. Jiang, S. D. Lin, *J. Mater. Chem. A* **2024**, *12*, 3659–3670.
[12] Y. Zhang, X. Guo, Q. Yang, Y. Shao, Y. Du, J. Qi, M. Zhao, Z. Shang, Y. Hao, Y. Tang, Y. Li, R. Zhang, B. Wang, J. Qiu, *Proc. Natl. Acad. Sci. U.S.A.* **2023**, *120*, e2314408120.
[13] B. Tong, Z. Song, H. Wan, W. Feng, M. Armand, J. Liu, H. Zhang, Z. Zhou, *InfoMat* **2021**, *3*, 1364–1392.
[14] Q. Yu, Y. Xiao, S. Zhao, Y. Miao, S. Wan, L. Zhou, J. Rong, G. Hou, S. Chen, *Adv. Funct. Mater.* **2024**, *34*, 2401868.
[15] D. Ouyang, J. Guan, X. Wan, B. Liu, C. Miao, Z. Wang, *ACS Appl. Mater. Interfaces* **2024**, *16*, 42894–42904.

Manuscript received: December 11, 2024
Revised manuscript received: January 26, 2025
Accepted manuscript online: February 5, 2025
Version of record online: February 19, 2025